Pergamon

Int. J. Heat Mass Transfer. Vol. 37, No. 17, pp. 2799–2808, 1994

0017-9310/94 $7.00+0.00

0017-9310(94)E0075-6

Femtosecond laser heating of multi-layer metals—II. Experiments

T. Q. QIU,† T. JUHASZ,‡ C. SUAREZ,‡ W. E. BRON‡ and C. L. TIEN†§

†Department of Mechanical Engineering, University of California, Berkeley, CA 94720, U.S.A.
‡Department of Physics, University of California, Irvine, CA 92717, U.S.A.

(*Received* 2 *February* 1993)

Abstract—Femtosecond thermoreflectivity experiments are performed to investigate energy deposition and transport during the very early period of short-pulsed laser heating of gold and chromium multi-layer metal films. The chromium layer underneath the top gold layer is found to produce significant effects on the laser-energy deposition process. Experimental results show that radiation absorption by free electrons and the subsequent heating of the lattice occur not only at different times but also at different locations in a multi-layer metal film. The conventional radiation heating model fails to predict these results, and a more rigorous two-step model agrees well with the measured data.

INTRODUCTION

RADIATION deposition of energy in materials is a fundamental phenomenon central to laser diagnostics and laser processing. It converts radiation energy into material's internal energy, which initiates many thermal phenomena, such as heat pulse propagation, melting, evaporation and ablation. The operation of many laser techniques requires an accurate understanding and control of the energy deposition and transport processes. Examples include laser diagnostics of thin films [1, 2], laser processing of microstructures [3] and laser deposition of thin films [4]. Conventionally, the energy conversion process is assumed to take place instantaneously where radiation energy is absorbed [5]. The preceding paper (Part I) shows that this assumption may not be valid during short-pulse laser heating of multi-layer metals. The purpose of the present paper (Part II) is to investigate this assumption experimentally.

Recently, radiation deposition and the subsequent energy transport in homogeneous metals have been investigated with picosecond and femtosecond resolutions [6–12]. Results show that during high-power and short-pulse laser heating free electrons can be heated to an effective temperature much higher than the lattice temperature, which in turn leads to both a much faster energy propagation process and a much smaller lattice-temperature rise than those predicted from conventional radiation heating model. Corkum *et al.* [13] found that this electron-lattice nonequilibrium heating mechanism can significantly increase the resistance of molybdenum and copper mirrors to thermal damage during high-power laser irradiation when the laser pulse duration is shorter than one nanosecond. Nonequilibrium laser heating in multi-layer films, however, has not been studied experimentally.

Clemens *et al.* [14] studied thermal transport in multi-layer metals during picosecond laser heating. The measured temperature response in the first twenty picoseconds was found to be different from predictions of the conventional Fourier model. Due to the relatively low temporal resolution of the experiment (~4 ps), however, it is difficult to determine whether this difference is the result of nonequilibrium laser heating or from other heat conduction mechanisms, such as non-Fourier heat conduction [15], or reflection and refraction of thermal waves at interfaces [16]. Experiments with a higher temporal resolution are thus necessary to investigate mechanisms of energy deposition and transport in multi-layer metals during the very early period of laser heating.

EXPERIMENTAL SYSTEM

High-speed temperature measurement techniques play a critical role for a better understanding of novel phenomena and better control of processing that involves rapid temperature changes. Examples include rapid melting [17], superheating [18], femtosecond evaporation [19], laser annealing [20] and rapid thermal processing of thin films [21]. The overall temporal resolution of a temperature measurement system is often determined by the response time of detectors. For example, the response time of a micro thermal sensor and a high-speed photodetector is typically limited to microseconds [22] and picoseconds [23], respectively. When the time period of a thermal process is in the range of picoseconds or shorter, the entire measurement of a single thermal event becomes intractable, and a repetitive type measurement tech-

§Author to whom correspondence should be addressed.

NOMENCLATURE

C	heat capacity [J m^{-3} K^{-1}]
G	electron–lattice coupling factor [W m^{-3} K^{-1}]
I	intensity of laser beam [W m^{-2}]
L	film thickness [m]
N	number of photon-excited electrons
R	surface reflectivity
S	source term [W m^{-3}]
t	time [s]
t_p	laser pulse duration [s]
T	temperature [K]
T_e	effective electron temperature [K]
T_l	effective lattice temperature [K].

Greek symbols

κ	thermal conductivity [W m^{-1} K^{-1}]
τ	time delay [s].

nique, often called the pump-and-probe technique, must be used [6, 24].

In the pump-and-probe technique, an intense light pulse (pump pulse) is used to heat the material, and then a second pulse (probe pulse) with a preset time delay is used to detect the signal. During a thermal process, only one data point is collected and its temporal position is determined by the time delay between the pump and probe pulses. By repeating the measurement with different delay times in many identical thermal processes, a statistical picture of the transient process can be constructed.

In this work, a femtosecond laser is used to construct a pump-and-probe measurement system. Figure 1 shows the femtosecond laser system [25]. It contains a solid-state laser and a dye laser. A continuously pumped, actively mode-locked Nd : YAG laser is used as the master oscillator that delivers pulses of about 100 ps (10^{-10} s) duration at 1.06 μm wavelength with a 76 MHz repetition rate. After frequency doubling by a nonlinear optical crystal, the laser pulse wavelength is 532 nm at a power of 1 W (13 nJ per pulse). The 532 nm laser pulses are then used to synchronously pump a linear-cavity dye laser which generates femtosecond pulses [25]. The output of the dye laser is 100 fs (100×10^{-15} s) pulses with 80 mW of power (1.1 nJ per pulse), and has a wavelength around 630 nm.

Figure 2 is a schematic diagram of the experimental system. The laser pulses from the femtosecond laser system are separated into two beams with an intensity ratio of 9 : 1 by a beam splitter. The intense beam (pump beam) is used to heat the sample. It passes through a light modulator, which modulates the beam intensity at 1.2 MHz, and is then focused onto the sample surface by a microscope lens. The focal spot diameter is 5 μm and the laser pulse energy is 0.27 nJ.

The weak beam (probe beam) is used to measure reflectivity changes. Its intensity is about one-tenth of the pump beam so that it does not disturb the thermal process. The probe beam is reflected by a mirror mounted on a variable optical delay stage. A change of the mirror position varies the difference of the optical path length between the pump beam and the probe beam, which in turn varies the time delay between the pump pulse and probe pulse [26]. For example, a 300 μm difference in the optical path length generates a one picosecond (10^{-12} s) time delay. The mirror is driven by a computer controlled stepping motor. Every motor step moves the mirror by 5 μm,

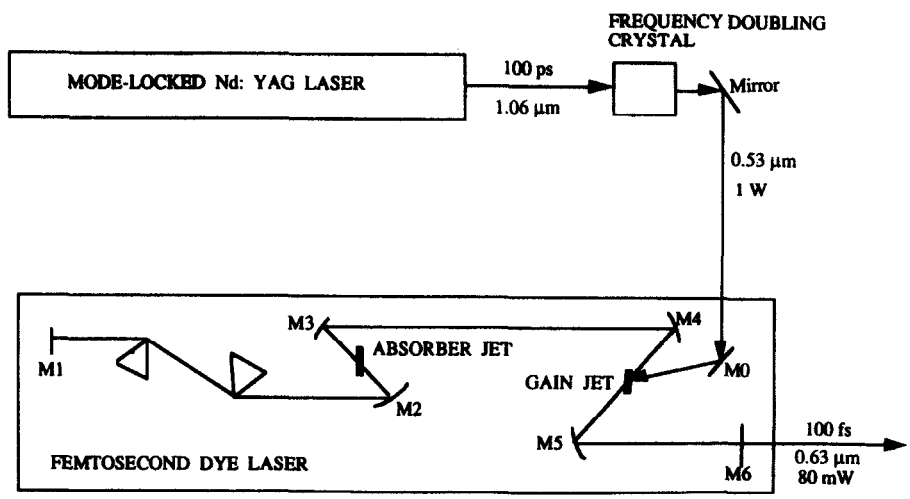

FIG. 1. Schematic diagram of the femtosecond laser system.

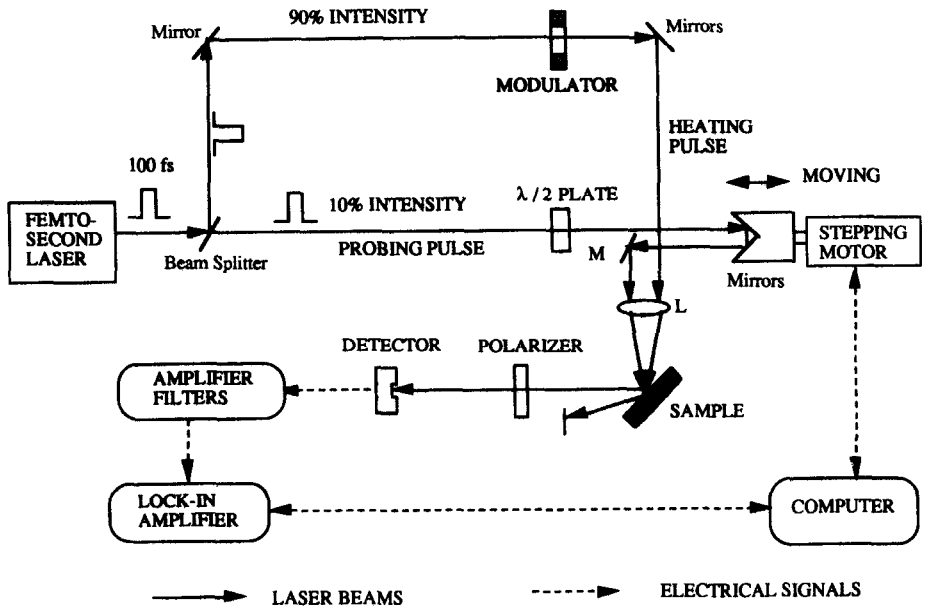

FIG. 2. Schematic diagram of the experimental system.

which varies the time delay by 33 fs. The polarization of the probe beam is rotated to be orthogonal to the pump beam by a half-wavelength plate so that the scattered pump beam can be blocked by a linear polarizer in front of the detector. Table 1 summarizes the experimental conditions.

MEASUREMENTS OF REFLECTIVITY CHANGES

Figure 3 shows a schematic diagram for the measurement principle of reflectivity changes during femtosecond laser pulse heating. The pump beam is modulated at a 1.2 MHz repetition rate, creating about 0.4 μs long heating pulse trains. Each heating train contains 32 individual 100 fs heating pulses separated by 13 ns (Fig. 3a). Each 100 fs heating pulse produces a femtosecond heating event. Since the time interval between two successive heating processes (13 ns) is much longer than the heating and heat relaxation periods, the two heating processes are independent events (Fig. 3b). Each heating process causes a transient variation of reflectivity from its reference value, R_0 (Fig. 3c). Following the heating train is a period (417 ns) without heating pulses. The probe pulses have a short time delay ($\tau = 0$–5 ps) related to the heating pulses (Fig. 3d). A train of the probe pulses is reflected by the sample at a reflectivity $R(\tau)$, and the subsequent train is reflected at the reference reflectivity R_0, resulting a periodic signal that has the same frequency and phase as the light modulator (Fig. 3e). The reflected probe beam is detected by a high-speed photodiode. Since the rise and fall time of the

Table 1. Experimental conditions

Device/laser beam	Parameter	Specification
Laser	Wavelength	630 nm
	Pulse duration	100 fs
	Pulse repetition rate	76 MHz
Beam modulator	Modulation frequency	1.2 MHz
Heating beam	Power	20 mW
	Pulse energy	0.266 nJ pulse^{-1}
	Focal spot diameter	~ 5 μm
Probe beam	Power	3.5 mW
	Pulse energy	0.046 nJ pulse^{-1}
	Focal spot diameter	~ 5 μm
Stepping motor	Range of time delay	-100 ps to 100 ps
	Resolution of time delay	33 fs step^{-1}
Detector	Type	PIN-type
	Response time	~ 10 ns
	Equivalent power of noise	5.8×10^{-9} W
	Minimum detectable $\Delta R/R$	1.7×10^{-6}
Lock-in amplifier	Time constant	0.1 s
	Frequency	1.2 MHz

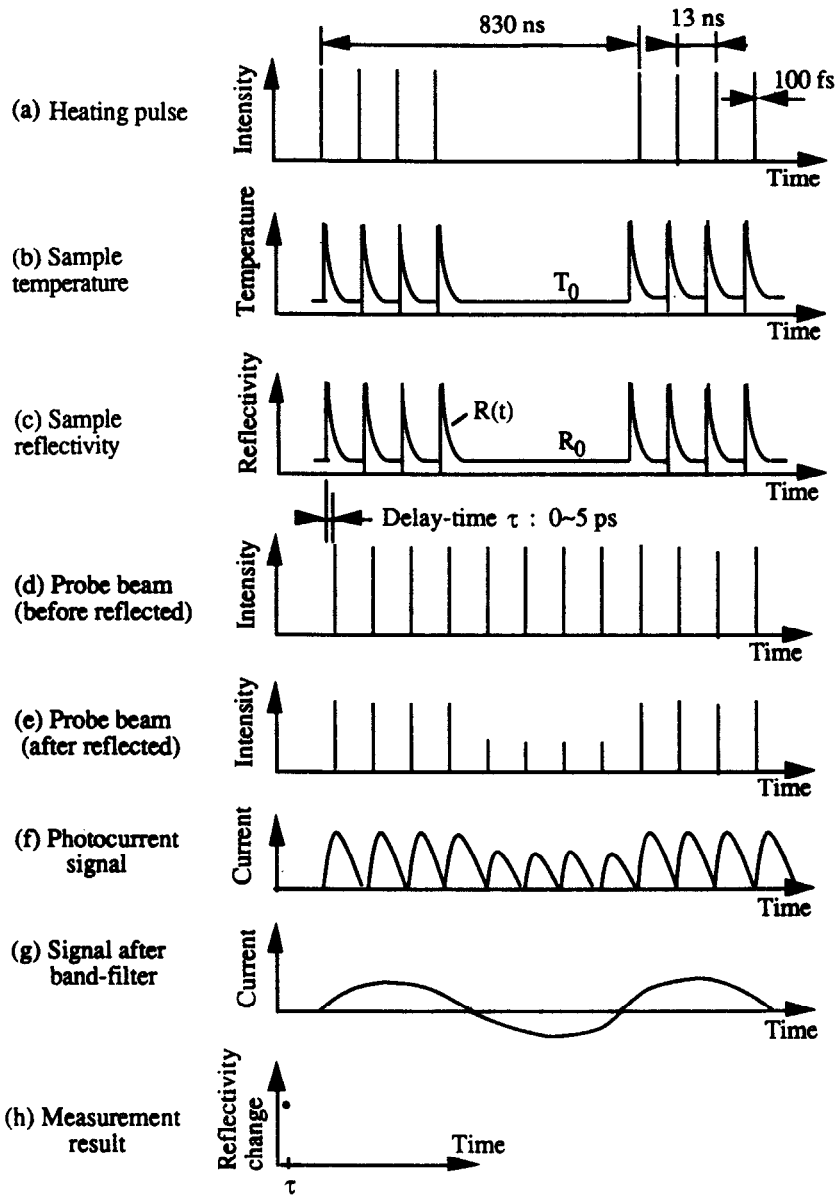

FIG. 3. Measurement principles for reflectivity changes.

photodiode (~ 10 ns) is much longer than the duration of laser pulses (100 fs), the photodetector functions like an integrating detector, producing a prolonged photo-current response after the arrival of each probe pulse. On the other hand, the photodiode's response time (~ 10 ns) is much shorter than the modulation period (0.83 μs); thus it can still resolve the modulated signal (Fig. 3f). Figure 3g shows the AC signal after the photo-current has passed through a narrow-band filter. The amplitude of the AC signal is proportional to the averaged reflectivity change, $\Delta R(\tau) = R(\tau) - R_0$. After calibrating the correlation between ΔR and the AC signal amplitude, the reflectivity change at a specific delay time, τ, during laser heating can be deduced (Fig. 3h). By varying the delay time, τ, and repeating the same measurement procedure, the entire reflectivity response during a laser heating process can be constructed.

RESULTS AND DISCUSSION

Laser pulse duration

The laser pulse duration varies on a day-to-day basis due to the aging of the laser dyes. Figure 4 shows a schematic diagram of the experimental system for the pulse duration measurement. It uses the laser pulse to measure itself [26]. A laser pulse is separated into two pulses that undergo different optical paths. When they are focused on a nonlinear frequency-doubling crystal, a time delay, τ, exists between them. The intensity of the frequency doubled light is

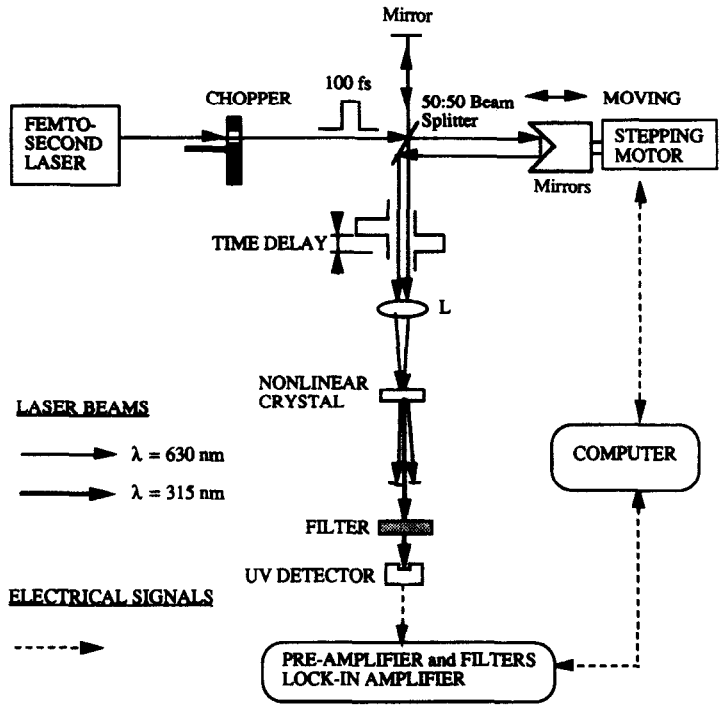

FIG. 4. Experimental system for the measurement of pulse auto-correlation.

$$I_s(t,\tau) = C \cdot I(t) \cdot I(t+\tau) \tag{1}$$

where $I(t)$ and $I(t+\tau)$ are the transient intensities of the two incident pulses and C is a crystal constant. Since the detector's response time is much larger than the laser pulse duration, the measured light intensity I_s is the auto-correlation of the laser pulse,

$$I_s(\tau) = C\int_{-\infty}^{+\infty} I(t)I(t+\tau)\,dt. \tag{2}$$

The temporal intensity distribution of femtosecond laser pulses is often assumed to be a hyperbolic-secant-squared pulse shape [25], which is very close to the Gaussian shape [26]. In this work, laser pulse shape is approximated by the Gaussian profile because of its simplicity, i.e.

$$I(t) = I_0 \exp(-4\ln 2 \cdot (t/t_p)^2). \tag{3}$$

Then the normalized detected signal is

$$\frac{I_s(\tau)}{I_s(0)} = \exp(-2\ln 2 \cdot (t/t_p)^2) \tag{4}$$

where t_p is the full-width-at-half-maximum (FWHM) pulse duration.

Figure 5 presents the measured auto-correlation of the laser pulse as well as the calculated results with different t_p. The comparison shows that the center of the pulse is Gaussian but the leading and trailing edges of the pulse are no longer Gaussian. The best fit of the Gaussian part gives a pulse duration $t_p = 100$ fs.

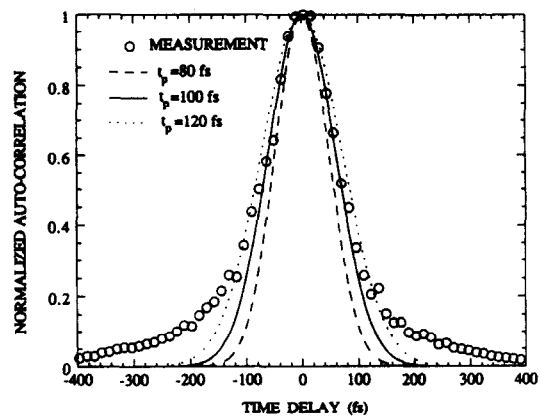

FIG. 5. Auto-correlation of laser pulses.

Reflectivity–temperature correlation

In general, reflectivity changes of metals are the results of the variations of electron distributions and are related to the parameters that characterize the electron system. In the present experiment, the initial laser heating results in a change in the occupation number of the electrons near the Fermi level, which is probed through measuring the transient reflectivity of the samples [6]. Fann *et al.* [10, 11] measured the electron distribution functions during femtosecond laser heating. The results show that, after a few hundred femtoseconds of the initial laser heating, electrons follow thermal equilibrium distributions and the electron system can thus be described by an effective

electron temperature, T_e. In the first few hundred femtoseconds, T_e is an approximated temperature; and, after this initial period, T_e represents a real electron temperature, which is not in general equal to the effective lattice temperature, T_l. The measured reflectivity change, ΔR, is related to the variation of the effective electron temperature, ΔT_e.

Rosei *et al.* [27–30] developed a quantum-mechanical model to characterize the temperature dependence of optical proprieties of noble metals. Figure 6 shows spectrally dependent reflectivity changes in a 0.1 μm thick gold film during 65 fs laser pulse heating. The theoretical results are calculated using Rosei *et al.*'s reflectivity model [27–30] and Anisimov *et al.*'s parabolic two-step laser heating model [31], which was also referred to as the two-temperature diffusion model [9, 13]. The experimental data are from Schoenlein *et al.* [32]. The model predicts qualitatively correct spectral dependence. At short laser wavelengths, an increase in the electron temperature results in an increase in the reflectivity. On the other hand, at long laser wavelengths, the temperature dependence is reversed. The predicted magnitude of reflectivity changes, however, is much larger than that measured, which might be due to the uncertainty of model parameters [33] and neglect of many important factors in the model, such as voids and lattice defects in the samples [34].

Figure 7 presents the predicted change of reflectivity as a function of the electron temperature by using Rosei *et al.*'s reflectivity model [27–30]. The reference temperature is 300 K. It shows that, in the regime 300 K $< T_e <$ 700 K, ΔR is approximately proportional to ΔT_e, which is consistent with Juhasz *et al.*'s results [9] that at relatively high temperatures (e.g. room temperature) ΔR is proportional to ΔT_e. Since the maximum electron temperature in this experiment is less than 700 K, the measured reflectivity-change can be assumed to be proportional to the electron-temperature change. Furthermore, the maximum

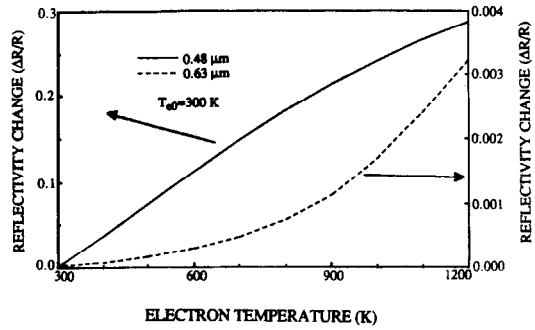

FIG. 7. Predicted correlation between reflectivity changes and temperature variations for gold.

reflectivity change $(\Delta R)_{max}$ is observed to be proportional to the laser fluence [7, 8, 32]. Likewise, the maximum electron-temperature change $(\Delta T_e)_{max}$ is roughly proportional to laser fluence in the energy range of the experimental observations (Fig. 8), as predicted from the parabolic two-step radiation heating model [31, 35]. Therefore, $(\Delta R)_{max}$ is also roughly proportional to $(\Delta T_e)_{max}$. As a result, the normalized

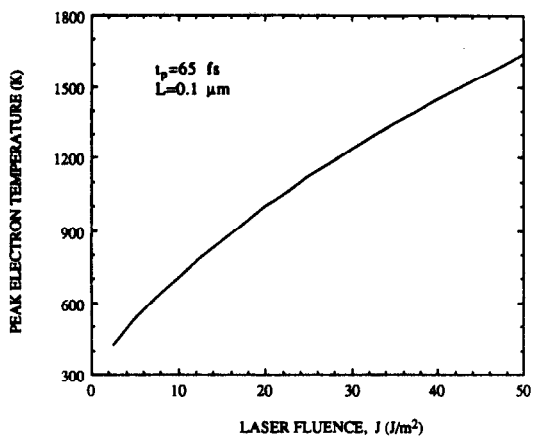

FIG. 8. Peak electron temperatures at various laser fluence.

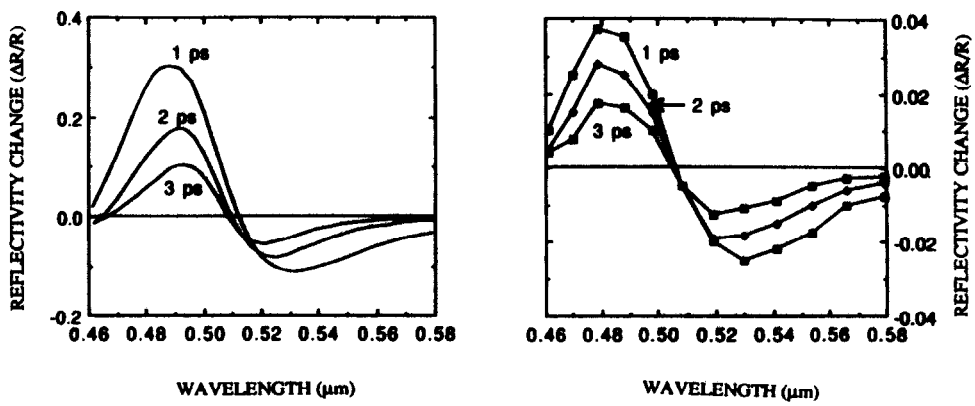

(a) Model (b) Experiment [32]

FIG. 6. Spectrally dependent reflectivity change during femtosecond laser heating of a gold film ($L = 0.1$ μm, $J = 40$ J m^{-2}, and $t_p = 65$ fs).

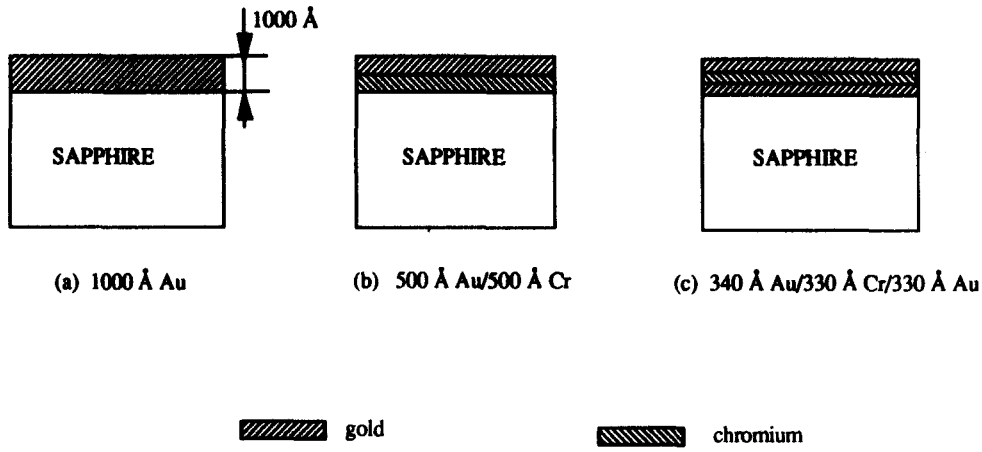

FIG. 9. Schematic diagram of multi-layer samples.

electron-temperature change can be deduced from the measured reflectivity-change as

$$\frac{\Delta T_e}{(\Delta T_e)_{max}} \approx \frac{\Delta R_e}{(\Delta R_e)_{max}}. \tag{5}$$

Laser heating of multi-layer metals

The samples are single-layer, double-layer and triple-layer gold and chromium thin films deposited on sapphire substrates (Fig. 9). The samples were processed in the U.C. Berkeley Microfabrication Laboratory by thermal evaporation. The film deposition pressure is $2\text{–}4\times10^{-6}$ torr and the growth rate is around 5 Å s^{-1}. The thickness is measured simultaneously during the film deposition process by a crystal monitor to an accuracy of 10 Å. The double-layer samples contain a 500 Å thick gold layer on the top of a 500 Å thick chromium layer. The triple layer samples have a sandwich structure with 340 Å gold on top, 330 Å gold at the bottom, and 330 Å chromium in between. The deposition temperature is below 300°C; thus gold and chromium do not form an alloy at their interface during the film deposition process.

Figure 10 shows the comparison of experimental results with predicted electron-temperature changes at the front surface of a single-layer 200 Å thick gold film during 100 fs laser pulse heating. Two models considered in the comparison are the parabolic one-step radiation heating model (POS),

$$C\frac{\partial T}{\partial t} = \nabla\cdot(\kappa\nabla T) + S \tag{6}$$

and the parabolic two-step radiation heating model (PTS),

$$C_e(T_e)\frac{\partial T_e}{\partial t} = \nabla\cdot\left(\frac{T_e}{T_l}\kappa\nabla T_e\right) - G(T_e - T_l) + S \tag{7}$$

$$C_l\frac{\partial T_l}{\partial t} = G(T_e - T_l) \tag{8}$$

where T_l is the lattice temperature, C_e and C_l are the electron and the lattice heat capacities, respectively, S is the laser heating source term, and G is the electron–lattice coupling factor. The POS model is based on the empirical Fourier heat conduction law and the assumption that radiation energy is deposited directly into the lattice where it is absorbed. The PTS model considers a microscopic two-step radiation heating process: radiation absorption by electrons and the subsequent energy redistribution between electrons and the metal lattice. The ratio of the electron temperature to the lattice temperature in the PTS model accounts for the effect of electron–lattice non-equilibrium heating on the electron thermal conductivity [36]. Detailed discussion about different radiation heating models and material properties used in the model predictions has been presented in the preceding paper (Part I). Predictions from the PTS model, which involve no fitting parameters, agree well with the experimental results, revealing a rapid electron heating process and a subsequent slow electron–lattice thermalization process. The POS model fails to predict the thermalization process.

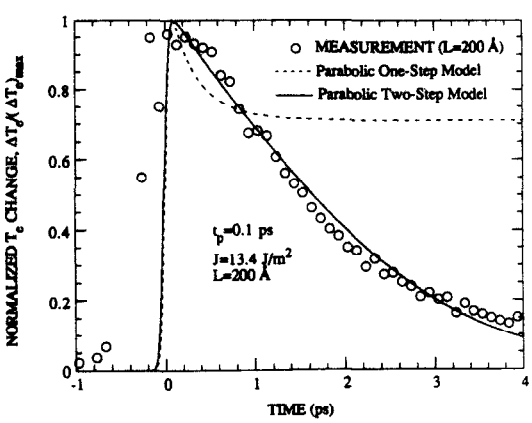

FIG. 10. Comparison of experimental results with predicted transient electron-temperature changes.

Figure 11 shows effects of film thickness on the transient electron–temperature response at the front surface of single-layer gold films during 100 fs laser pulse heating. Since the radiation penetration depth

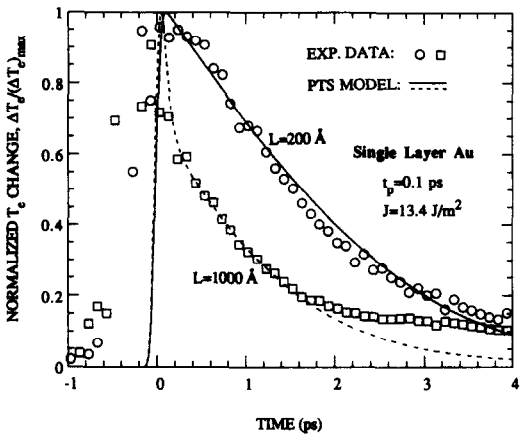

FIG. 11. Effects of film thickness on the transient electron-temperature response.

in gold at 630 nm wavelength is around 150 Å, the laser energy deposits itself in the 150 Å thick film volumetrically, resulting in a quite uniform temperature distribution. Therefore, there is a very limited transport effect in the 200 Å film. On the other hand, for the 1000 Å thick film, since the radiation penetration depth is much smaller than the film thickness, electrons can carry the absorbed energy away from the radiation absorption region rapidly, resulting in a more rapid surface temperature drop. This is consistent with previously reported experimental results [7, 8, 37]. The predictions of the PTS model agree well with the measurements.

Figure 12 presents the comparison of the experimental results with the predicted electron-temperature response at the front surface of multi-layer films from the conventional POS model during 100 fs laser pulse heating. In the POS model, the laser energy is deposited directly into the gold lattice and then the absorbed energy propagates slowly away from the radiation absorption region. For example, the thermal diffusivity of gold is 1.2×10^{-4} m^2 s^{-1}; thus it takes about 6 ps for a heat pulse to diffuse a 300 Å distance. During the femtosecond laser heating process, the heat pulse does not travel far enough to reach the gold–chromium interface and feel the existence of the other layers. Therefore the POS model predicts the same thermal response in films with different structures. This prediction does not agree with the experimental observation, which clearly shows the film-structure-dependent responses.

Figure 13 shows the comparison of measured results with predictions from the PTS model during 100 fs laser pulse heating of multi-layer films. Predictions from the PTS model agree with experimental results. Unlike the conventional POS model, which fails to predict the structure-dependent radiation deposition process, the PTS model shows that the laser heating process is very sensitive to the existence of the chromium layer underneath the top gold coating layer. In the PTS model the laser energy is initially deposited into the free electrons in the top gold layer. Before electrons transfer the absorbed energy to the lattice, they can move very rapidly away from the radiation absorption region. Since the heat capacity of free electrons is two orders of magnitude smaller than that of the lattice, the heat diffusion process by pure electrons is much faster than that by the thermal equilibrium electrons and the lattice. For example, the thermal diffusivity of electrons in gold is 1.5×10^{-2} m^2 s^{-1} (Part I). It takes only about one hundred femtoseconds for the heat pulse to propagate across the top gold layer and reach the underlying chromium layer. Since chromium has different material properties from gold, the chromium layer is expected to affect the thermal response of the top gold coating.

Since electrons have a lower thermal diffusivity in chromium, 1.6×10^{-3} m^2 s^{-1} (Part I), than that in gold (1.5×10^{-2} m^2 s^{-1}), the chromium layer slows down the thermal diffusion process. On the other hand, chromium has a much larger electron–lattice coupling factor than gold [35, 38]. Therefore, electrons can transfer energy to the lattice much more rapidly in chromium than in gold. The chromium layer acts like an electron heat sink, removing energy from the electron system in the top gold layer to the lattice system in the underlying chromium layer. As a result, the surface electron temperature drops more rapidly in

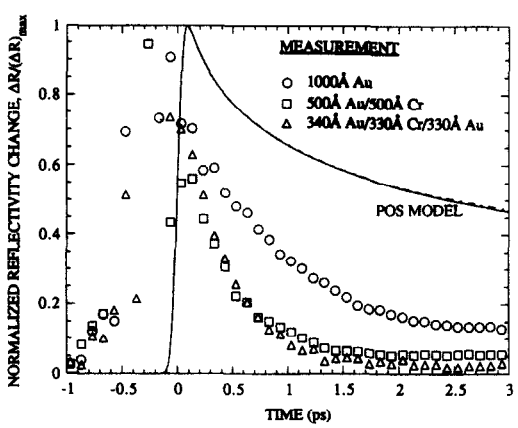

FIG. 12. Comparison of measured results with predictions from the conventional POS model.

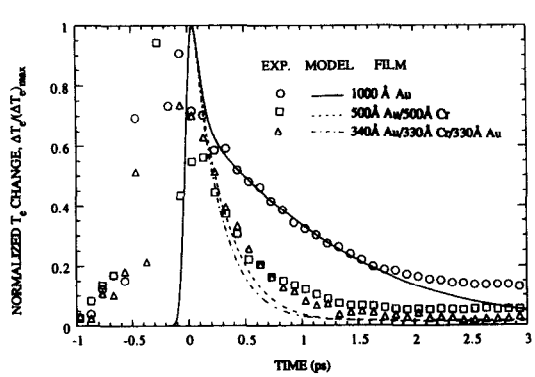

FIG. 13. Comparison of measured results with predictions from the PTS model.

the multi-layer films than in the single-layer film. Consequently, electrons transfer the majority of the absorbed laser energy to the underlying chromium lattice instead of to the top layer gold lattice, reducing the rise of the peak lattice temperature of the gold coating layer. This mechanism could be utilized to optimize temperature distributions in mirror coatings to enhance their resistant to thermal damage in high-power laser applications. The surface electron-temperature response of gold–chromium double-layer films and the gold–chromium–gold triple-layer films are very close, indicating that the additional layer in the triple-layer sample does not strongly affect the energy deposition and transport process.

Experimental uncertainty

The noise in the photon detecting process determines the smallest detectable reflectivity-change. The equivalent radiation power of the detector's noise is 5.8×10^{-9} W at 630 nm wavelength and 76 MHz band width [39]. Since the probe beam power is 3.5 mW, the minimum detectable reflectivity-change is $(\Delta R/R)_{\min} = 5.8 \times 10^{-9}$ W/3.5 mW $= 1.7 \times 10^{-6}$ for this measurement system.

The ultimate limit of the detectable reflectivity change is set by the quantum shot noise caused by the fluctuation in the number of photon-excited electrons in the detector. In this experiment, the signal processing time (i.e. the time constant of the lock-in amplifier) is 0.1 s, and the number of photons received by the detector in this time period is in the order of 7×10^{13}. The detector can convert 42% photons to photo-electrons [39]; thus the number of photon-excited electrons is $N = 3 \times 10^{13}$. The RMS fluctuation of the electron number is $N^{1/2} = (3 \times 10^{13})^{1/2} = 5.5 \times 10^{6}$. This fluctuation sets the fundamental limit on the minimum detectable reflectivity-change as $N^{1/2}/N = 5.5 \times 10^{6}/3 \times 10^{13} = 1.8 \times 10^{-7}$. The reflectivity-change in the experiment is in the range of 10^{-3} to 10^{-5}, and thus it can be well detected.

At the very early period of laser heating, the signal is noisy. Groeneveld [12] suggested that the noise is due to the interference between the pump laser pulse and the probe laser pulse, and a smoother sample surface could reduce the noise level. Substrates with different surface roughness have been used in the current experiments, including sapphire disks and standard silicon wafers. The silicon wafers have smoother surfaces than the sapphire disks; however, the noise level observed from the samples deposited on the silicon wafers is much higher than that observed from the samples deposited on the sapphire disks, indicating there might be other substrate-dependent sources of noise.

CONCLUSIONS

Time-resolved experiments on the femtosecond scale have been conducted to investigate energy deposition and transport during short-pulse laser heating of gold and chromium multi-layer metals. The temporal resolution of the measurement system is 100 fs, which provides the capability to investigate the initial energy transport process in multi-layer metals. Predictions from the two-step radiation heating model agree well with experimental data, but the conventional one-step model fails to even predict the correct trend of the thermal responses, suggesting that microscopic radiation deposition processes and electron–lattice interactions must be considered for short-pulse laser applications. Both the experimental results and the two-step model predictions show a strong dependence of thermal response of thin metal films on their structures. The chromium layer beneath the top gold layer can enhance the rate of energy removal from free electrons of the top gold coating to the lattice of the underlying chromium layer, which in turn reduces the lattice temperature rise of the coating layer. This mechanism could be utilized to increase the resistance of mirror coatings to thermal damage in high-power laser applications.

Acknowledgements—The authors acknowledge the financial support from the U.S. National Science Foundation, the U.S. Department of Energy, and the K. C. Wang Education Foundation in Hong Kong.

REFERENCES

1. J. Opsal, The application of thermal wave technology to thickness and grain size monitoring of aluminum films, in *Metallization: Performance and Reliability Issues for VLSI and ULSI*, SPIE Vol. 1596, pp. 120–131 (1991).
2. A. Mandelis and S. B. Peralta, Thermal-wave based materials characterization and nondestructive evaluation of high-temperature superconductors: a critical review. In *Physics and Materials Science of High Temperature Superconductors* II (Edited by R. Kossowsky *et al.*), pp. 413–440. Kluwer Academic Publishers, Boston, MA (1992).
3. C. P. Grigoropoulos, Heat transfer in laser processing of thin films, *Ann. Rev. Heat Transfer* V, pp. 77–130. Hemisphere, New York (1994).
4. J. T. Cheung and H. Sankur, Growth of thin films by laser-induced evaporation, *CRC Crit. Rev. Solid State Mater. Sci* **15**, 63–109 (1988).
5. R. Siegel and J. R. Howell, *Thermal Radiation Heat Transfer* (3rd Edn). Hemisphere, Washington, DC (1992).
6. G. L. Eesley, Observation of nonequilibrium electron heating in copper, *Phys. Rev. Lett.* **51**, 2140–2143 (1983).
7. S. D. Brorson, J. G. Fujimoto and E. P. Ippen, Femtosecond electronic heat-transfer dynamics in thin gold films, *Phys. Rev. Lett.* **59**, 1962–1965 (1987).
8. H. E. Elsayed-Ali, T. Juhasz, G. O. Smith and W. E. Bron, Femtosecond thermoreflectivity and thermotransmissivity of polycrystalline and single-crystalline gold films, *Phys. Rev. B* **43**, 4488–4491 (1991).
9. T. Juhasz, H. E. Elsayed-Ali, X. H. Hu and W. E. Bron, Time-resolved thermoreflectivity of thin gold films and its dependence on the ambient temperature, *Phys. Rev. B* **45**, 13819–13822 (1992).
10. W. S. Fann, R. Storz, H. W. K. Tom and J. Bokor, Direct measurement of nonequilibrium electron-energy distributions in sub-picosecond laser-heated gold films, *Phys. Rev. Lett.* **68**, 2834–2837 (1992).
11. W. S. Fann, R. Storz, H. W. K. Tom and J. Bokor,

Electron thermalization in gold, *Phys. Rev. B* **46,** 13592–13595 (1992).
12. R. H. M. Groeneveld, Femtosecond spectroscopy on electrons and phonons in noble metals, Ph.D thesis, Van der Waals—Zeeman Laboratory, University of Amsterdam (1992).
13. P. B. Corkum, F. Brunel and N. K. Sherman, Thermal response of metals to ultrashort-pulse laser excitation, *Phys. Rev. Lett.* **61,** 2886–2889 (1988).
14. B. M. Clemens, G. L. Eesley and A. C. Paddock, Time-resolved thermal transport in compositionally modulated metal films, *Phys. Rev. B* **37,** 1085–1096 (1988).
15. M. N. Ozisik and D. Y. Tzou, On the wave theory in heat conduction. In *Fundamental Issues in Small Scale Heat Transfer* (Edited by Y. Bayazitoglu and P. G. Peterson), HTD, Vol. 227, pp. 13–27. ASME, New York (1992).
16. D. Y. Tzou, Reflection and refraction of thermal waves from a surface or an interface between dissimilar materials, *Int. J. Heat Mass Transfer*, **36,** 401–410 (1993).
17. B. C. Larson, J. Z. Tischler and D. M. Mills, Nanosecond resolution time-resolved X-ray study of silicon during pulsed-laser irradiation, *J. Mater. Res.* **1,** 144–154 (1986).
18. J. W. Herman and H. E. Elsayed-Ali, Superheating of Pb (111), *Phys. Rev. Lett.* **69,** 1228–1231 (1992).
19. M. C. Downer, R. L. Fork and C. V. Shank, Femtosecond imaging of melting and evaporation at a photoexcited silicon surface, *J. Opt. Soc. Am. B* **2,** 595–599 (1985).
20. C. P. Grigoropoulos, R. H. Buckholz and G. A. Domoto, An experimental study on laser annealing of thin silicon layers, *J. Heat Transfer* **110,** 416–423 (1988).
21. K. Maex, Rapid thermal processing and thin film technologies, *Microelectronic Engineering* **15,** 467–474 (1991).
22. J. M. Hager, S. Simmons, D. Smith, S. Onishi, L. W. Langley and T. E. Diller, Experimental performance of a heat flux microsensor, *Journal of Engineering for Gas Turbines and Power* **113,** 246–250 (1991).
23. C. B. Johnson, Status of high-speed optical detector technologies at ITT/EOPD. In *Image Intensification*, SPIE Vol. 1072, pp. 2–12 (1989).
24. S. L. Shapiro (Ed.), *Ultrashort Light Pulses: Picosecond Techniques and Applications*, Springer, Berlin (1977).
25. T. Juhasz, G. O. Smith, S. M. Mehta, K. Harris and W. E. Bron, Generation and kilohertz rate amplification of synchronized femtosecond and picosecond laser pulses, *IEEE J. Quantum Electronics* **25,** 1704–1707 (1989).
26. E. P. Ippen and C. V. Shank, Techniques for measurement. In *Ultrashort Light Pulses: Picosecond Techniques and Applications* (Edited by S. L. Shapiro), pp. 83–122. Springer, Berlin (1977).
27. R. Rosei and D. W. Lynch, Thermomodulation spectra of Al, Au, and Cu, *Phys. Rev. B* **5,** 3883–3893 (1972).
28. R. Rosei, F. Antonangeli and U. M. Grassano, D bands position and width in gold from very low temperature thermomodulation measurements, *Surf. Sci.* **37,** 689–699 (1973).
29. R. Rosei, Temperature modulation of the optical transitions involving the Fermi surface in Ag: theory, *Phys. Rev. B* **10,** 474–483 (1974).
30. M. Guerrisi and R. Rosei, Splitting of the interband absorption edge in Au, *Phys. Rev. B* **12,** 557–563 (1975).
31. S. I. Anisimov, B. L. Kapeliovich and T. L. Perel'man, Electron emission from metal surfaces exposed to ultrashort laser pulses, *Sov. Phys. JETP* **39,** 375–377 (1974).
32. R. W. Schoenlein, W. Z. Lin, J. G. Fujimoto and G. L. Eesley, Femtosecond studies of non-equilibrium electronic processes in metals, *Phys. Rev. Lett.* **58,** 1680–1683 (1987).
33. N. E. Christensen and B. O. Seraphin, Relativistic band calculation and the optical properties of gold, *Solid State Commun.* **8,** 1221–1226 (1970).
34. D. E. Aspnes, E. Kinsbron and D. D. Bacon, Optical properties of Au: sample effects, *Phys. Rev. B* **21,** 3290–3299 (1980).
35. T. Q. Qiu and C. L. Tien, Short-pulse laser heating on metals, *Int. J. Heat Mass Transfer* **35,** 719–726 (1992).
36. T. Q. Qiu and C. L. Tien, Heat transfer mechanisms during short-pulse laser heating of metals, *J. Heat Transfer* **115,** 835–841 (1993).
37. H. E. Elsayed-Ali and T. Juhasz, Femtosecond time-resolved thermomodulation of thin gold films with different crystal structures, *Phys. Rev. B* **47,** 13599–13610 (1993).
38. S. D. Brorson, A. Kazeroonian, J. S. Moodera, D. W. Face, T. K. Cheng, E. P. Ippen, M. S. Dresselhaus and G. Dresselhaus, Femtosecond room-temperature measurement of the electron–phonon coupling constant λ in metallic superconductors, *Phys. Rev. Lett.* **64,** 2172–2175 (1990).
39. S. F. Jacobs, Nonimaging detectors. In *Handbook of Optics* (Edited by W. G. Driscoll and W. Vaughan), pp. 4–35. McGraw-Hill, New York (1978).